LDA+DMFT implemented with the pseudopotential plane-wave approach

2008 J. Phys.: Condens. Matter 20 135227

(http://iopscience.iop.org/0953-8984/20/13/135227)

J. Phys.: Condens. Matter **20** (2008) 135227 (7pp) doi:10.1088/0953-8984/20/13/135227

LDA + DMFT implemented with the pseudopotential plane-wave approach

G Trimarchi[1,2,4], **I Leonov**[1], **N Binggeli**[1,2], **Dm Korotin**[3] and **V I Anisimov**[3]

[1] Abdus Salam International Centre for Theoretical Physics, Trieste 34014, Italy
[2] Democritos National Simulation Center, INFM-CNR, Trieste I-34014, Italy
[3] Institute of Metal Physics, Russian Academy of Sciences, Ural Division, 620219 Yekaterinburg GSP-170, Russia

E-mail: binggeli@ictp.it

Received 21 December 2007, in final form 22 February 2008
Published 13 March 2008
Online at stacks.iop.org/JPhysCM/20/135227

Abstract

We present a joint implementation of dynamical-mean-field theory (DMFT) with the pseudopotential plane-wave approach, via Wannier functions, for the determination of the electronic properties of strongly correlated materials. The scheme uses, as input for the DMFT calculations, a tight-binding Hamiltonian obtained from the plane-wave calculations by projection onto atomic-centered symmetry-constrained Wannier functions for the correlated orbitals. We apply this scheme to two prototype systems: a paramagnetic correlated metal, $SrVO_3$, and a paramagnetic correlated system, V_2O_3, which exhibits a metal–insulator transition. Comparisons with available linear-muffin-tin-orbital (LMTO) plus DMFT calculations demonstrate the suitability of the joint DMFT pseudopotential plane-wave approach to describe the electronic properties of strongly correlated materials. This opens the way to future developments using the pseudopotential plane-wave DMFT approach to address total-energy properties, such as structural properties.

(Some figures in this article are in colour only in the electronic version)

1. Introduction

Dynamical electron correlations play an important role in the physics of strongly correlated electronic materials, in particular in determining the properties of their paramagnetic and ferromagnetic phases, as well as their metal–insulator transitions. The latter transitions are related to some of the most dramatic effects observed in transition-metal oxides, such as the colossal magnetoresistance effect in doped manganites [1, 2]. The properties of transition-metal oxides are also known to be controlled by a strong and complex interplay between electronic, magnetic, and structural degrees of freedom [2]. This interplay leads to giant responses to small changes in external parameters such as temperature, pressure, magnetic field, or doping, which makes such materials attractive for technological applications.

A new theoretical framework has made possible in recent years the incorporation of dynamical correlations in electronic structure calculations of strongly correlated materials [3–5]. It combines the dynamical-mean-field theory (DMFT) of many-body physics with density-functional electronic structure calculations in the local-density approximation (LDA), or in the generalized gradient approximation (GGA), and is commonly referred to as LDA + DMFT. So far LDA + DMFT computations have been generally implemented with the linear muffin-tin orbital (LMTO) method, and in some cases also with mixed-basis methods [7], which also incorporate atomic-like orbitals in the basis set. In view of the importance, however, of the interplay between structural and electronic properties in correlated oxides, it would be highly desirable to have a joint implementation of DMFT with the electronic structure pseudopotential plane-wave method. The latter method is indeed known to be well suited to address total-energy properties, such as structural properties. This is related to the plane-wave basis, in particular, which is independent of the atomic positions in the unit cell and whose completeness can be controlled by a single parameter, the plane-wave kinetic energy cutoff.

[4] Present address: National Renewable Energy Laboratory Golden, CO 80401, USA.

Recently, approaches based on Wannier functions have been proposed to carry out LDA + DMFT computations, using e.g. atomic-centered Wannier functions [6], or maximally localized Wannier functions [7], or Wannier functions constructed with the *N*th order muffin-tin-orbital method [8]. For strongly correlated materials, Wannier functions represent a convenient, physically sound set of localized orbitals for the correlated electrons that can be used to construct an interface between DMFT and LDA/GGA calculations. This is especially important for LDA/GGA methods which do not employ atomic-like basis functions, as is the case of the pseudopotential plane-wave method.

Here we present a joint implementation of DMFT with the pseudopotential plane-wave approach, and demonstrate its suitability to determine the electronic properties of correlated oxides. This is a prerequisite to address, in the future, also total-energy and structural properties. We use as input for the DMFT calculations a tight-binding Hamiltonian, $H^{\mathrm{TB}}(\mathbf{k})$, constructed from the pseudopotential plane-wave calculations using atomic-centered symmetry-constrained Wannier functions for the correlated orbitals. We apply this approach to two different test cases: a correlated paramagnetic metal, $SrVO_3$, with a simple cubic perovskite structure, and a correlated paramagnetic system, V_2O_3, which has a more complex trigonal crystal structure, and exhibits a Mott–Hubbard transition. To our knowledge, this is the first successful implementation of LDA + DMFT using the pseudopotential plane-wave approach.

2. Method

2.1. LDA + DMFT calculation scheme

The standard (although simplified[5]) scheme generally used to carry out LDA + DMFT calculations includes the following three steps.

First, an LDA/GGA self-consistent electronic structure calculation is performed for the crystal and phase of interest. The calculated bands associated with the relevant correlated orbitals (e.g. the transition-metal 3d-t_{2g} orbitals in our examples) are then mapped onto a **k**-dependent tight-binding Hamiltonian, $\widehat{H}^{\mathrm{TB}}_{\mathrm{LDA}}(\mathbf{k})$, where **k** is a vector of the crystal Brillouin zone (BZ). In practice, in the case of LDA/GGA calculations performed using, as a basis set, atomic-like orbitals, this Hamiltonian is readily obtained as:

$$\widehat{H}^{\mathrm{TB}}_{\mathrm{LDA}}(\mathbf{k}) = \sum_{m,m',\sigma} H^{\mathrm{TB}(\sigma)}_{mm'}(\mathbf{k}) c^{\dagger}_{\mathbf{k}m\sigma} c_{\mathbf{k}m'\sigma} \tag{1}$$

where $H^{\mathrm{TB}(\sigma)}_{mm'}(\mathbf{k})$ are the matrix elements, in a given **k** and σ spin-polarization subspace, of the LDA/GGA Hamiltonian between the relevant correlated atomic-like orbitals, indexed by m, m', and $c^{\dagger}_{\mathbf{k}m\sigma}$ ($c_{\mathbf{k}m\sigma}$) is the creation (annihilation) operator for an electron in orbital m with spin σ and wavevector **k**. As we are interested here in the case of paramagnetic phases, we will omit in the following the spin label σ in $H^{\mathrm{TB}(\sigma)}_{mm'}$. We note that, at the LDA/GGA level, the paramagnetic phase is simply modeled by a non-magnetic state. We are including in the sum, in equation (1), a minimal basis set of m, m' orbitals corresponding to the relevant on-site correlated orbitals near the Fermi energy. More generally, however, additional non-correlated orbitals may be included, when needed, to improve the description of the spectrum further away from the Fermi energy [9]. For simplicity, we will focus in the following on the case of periodic systems with a single type of correlated atomic site.

Next, the LDA/GGA tight-binding Hamiltonian is supplemented with on-site Coulomb interactions for the correlated orbitals in a many-body Hamiltonian of the form:

$$\begin{aligned}\widehat{H} = &\sum_{\mathbf{k},m,m',\sigma} H^{\mathrm{TB}}_{mm'}(\mathbf{k}) c^{\dagger}_{\mathbf{k}m\sigma} c_{\mathbf{k}m'\sigma} - \sum_{I,m,\sigma} \Delta\epsilon^{\mathrm{dc}} n_{Im\sigma} \\ &+ \sum_{I,m} U n_{Im\uparrow} n_{Im\downarrow} + \sum_{I,m\neq m',\sigma,\sigma'} (V - \delta_{\sigma\sigma'} J) n_{Im\sigma} n_{Im'\sigma'}.\end{aligned} \tag{2}$$

The index I labels the lattice sites, m, m' label the relevant correlated atomic orbitals, σ, σ' the spin states ($\uparrow$ and $\downarrow$), and $n_{Im\sigma}$ is the operator for the occupation of the correlated orbitals. The first term, on the right-hand side of equation (2), is the LDA/GGA part of the Hamiltonian. The second term is a double-counting correction, formally introduced to remove the on-site Coulomb interactions already present, in an average way, in the LDA/GGA Hamiltonian. In principle, the double-counting potential $\Delta\epsilon^{\mathrm{dc}}$ may be taken as [4]: $\Delta\epsilon^{\mathrm{dc}} = U(\bar{n} - \frac{1}{2})$, where $\bar{n}$ is the average occupation per correlated orbital. In practice, however, if one takes into account only d orbitals (or only f orbitals), the double-counting correction acts on the whole d(f) band and shifts it by $\Delta\epsilon^{\mathrm{dc}}$. This potential amounts thus to a rigid energy shift of the quasiparticle spectrum in the DMFT calculations. It can therefore be absorbed into the chemical potential, which in turn is determined by the number of electrons. Hence the actual value of $\Delta\epsilon^{\mathrm{dc}}$ has no influence on the spectral properties. The third and fourth terms, on the right-hand side of equation (2), are the interaction terms, where U is the on-site Coulomb repulsion parameter, J the Hund's rule exchange parameter, and $V = U - 2J$ [10].

Finally, the model Hamiltonian, in equation (2), is solved by means of DMFT. DMFT maps the lattice model onto an effective single-impurity problem subject to a self-consistent condition on the impurity self-energy, $\hat{\Sigma}(\epsilon)$, or, equivalently, on the local Green's function, $\hat{G}(\epsilon)$ [11]. This mapping represents an exact solution in the limit of infinite dimension of the lattice problem. The local impurity Green's function and self-energy matrices are related through:

$$\begin{aligned}G_{mm'}(\epsilon) = \frac{1}{\Omega_{\mathrm{BZ}}} \int \mathrm{d}\mathbf{k} ([(\epsilon - \mu)\mathbf{1} - \mathbf{H}^{\mathrm{TB}}(\mathbf{k}) \\ - \boldsymbol{\Sigma}(\epsilon)]^{-1})_{mm'},\end{aligned} \tag{3}$$

where m, m' label the correlated orbitals, μ is the chemical potential, $\mathbf{1}$, $\boldsymbol{\Sigma}(\epsilon)$, and $\mathbf{H}^{\mathrm{TB}}(\mathbf{k})$ are the unitary, self-energy, and LDA tight-binding-Hamiltonian matrices, respectively,

[5] LDA + DMFT calculations are presently performed using a non-self-consistent scheme. As has been proposed in [6] and [7], however, the charge density could be recalculated from the DMFT solution (Green's function) and injected into an iterative LDA + DMFT loop, to reach a self-consistent solution. In practice, however, this is a very demanding procedure, which to the best of our knowledge has not been successfully implemented so far.

and the integration extends over the BZ with volume $\Omega_{\rm BZ}$. Several different approaches may be used to solve the effective impurity problem, including the numerical renormalization group, exact diagonalization, the noncrossing approximation, and the Quantum Monte Carlo (QMC) method. In the present work, we employ, as impurity solver, the auxiliary fields QMC method of Hirsch and Fye [12]. For a given input impurity self-energy and Green's function matrices, the impurity solver yields a new set of Green's function and self-energy matrices [11]. The DMFT equations are solved in an iterative self-consistent cycle, until self-consistency is reached.

2.2. Tight-binding Hamiltonian from pseudopotential plane-wave calculations

Wannier functions provide a physically sound basis set to construct model Hamiltonians for correlated electrons. In the case of LDA/GGA plane-wave calculations, they also represent a practical route to build $\hat{H}^{\rm TB}_{\rm LDA}(\mathbf{k})$, given the delocalized nature of the basis functions.

The Wannier functions are obtained here using the approach by Ku *et al* [13]—inspired from the work by Marzari and Vanderbilt [14], to obtain atomic-centered Wannier functions with a given symmetry. First, a set of M trial functions are generated from the (pseudo) atomic wavefunctions of the correlated orbitals: $|\varphi_{m\mathbf{k}}\rangle = \sum_{\mathbf{R}} {\rm e}^{{\rm i}\mathbf{k}\mathbf{R}}|\varphi_m^{\mathbf{R}}\rangle$, where $\mathbf{R}$ are the lattice translation vectors and $|\varphi_m^{\mathbf{R}}\rangle$ are the atomic (pseudo) wavefunctions, in the unit cell $\mathbf{R}$, with a given symmetry. A set of M non-orthogonal Wannier functions (WF) in $\mathbf{k}$ space (or tight-binding Wannier functions) is then obtained by projecting these trial functions onto a set of Bloch functions, $|\psi_{j\mathbf{k}}\rangle$, belonging to a chosen (correlated bands) subspace:

$$|\widetilde{W}_{m\mathbf{k}}\rangle = \sum_{j=N_1}^{N_2} \langle\psi_{j\mathbf{k}}|\varphi_{m\mathbf{k}}\rangle|\psi_{j\mathbf{k}}\rangle. \tag{4}$$

The sum is over a Bloch subspace defined by imposing either some fixed band numbers, $N_1 \leqslant j \leqslant N_2$, or an energy window, $E_1 \leqslant \epsilon_j(\mathbf{k}) \leqslant E_2$, for the electronic bands $\epsilon_j(\mathbf{k})$. These Wannier functions are then orthogonalized, by diagonalizing their overlap matrix $O_{mm'}$, yielding a set of M orthogonalized Wannier functions: $|W_{m\mathbf{k}}\rangle = \sum_{m'}(O^{-1/2})_{mm'}|\widetilde{W}_{m'\mathbf{k}}\rangle$.

Using this basis set of Wannier functions, the tight-binding Hamiltonian matrix is given by:

$$H^{\rm TB-WF}_{mm'}(\mathbf{k}) = \sum_{j=N_1}^{N_2} \langle W_{m\mathbf{k}}|\psi_{j\mathbf{k}}\rangle\langle\psi_{j\mathbf{k}}|W_{m'\mathbf{k}}\rangle\epsilon_j(\mathbf{k}), \tag{5}$$

and can be used, in place of $H^{\rm TB}_{mm'}(\mathbf{k})$, in the many-body Hamiltonian, in equation (2). It should be noted that the conventional, real-space (lattice-site related) Wannier functions, $|W_m^{\mathbf{R}}\rangle$, are simply the Fourier transforms of the tight-binding Wannier functions: $|W_m^{\mathbf{R}}\rangle = \frac{1}{N_k}\sum_{\mathbf{k}} {\rm e}^{-{\rm i}\mathbf{k}\mathbf{R}}|W_{m\mathbf{k}}\rangle$. Only the tight-binding Wannier functions, however, are explicitly needed in the implementation.

We implemented this scheme to construct $H^{\rm TB}(\mathbf{k})$, in $\mathbf{k}$ space, in the framework of the pseudopotential plane-wave method. This was done as an interface between the Quantum-Espresso pwscf package [15] and the QMC-DMFT code. The matrix elements $\langle\psi_{j\mathbf{k}}|\varphi_{m\mathbf{k}}\rangle$, in equation (4), can be conveniently evaluated in reciprocal space, in the pseudopotential plane-wave scheme. For the trial wavefunctions $|\varphi_{m\mathbf{k}}\rangle$, we generated wavefunctions belonging to the point-group representations of the correlated atomic site. This was done by diagonalizing the occupation matrix [16]—calculated in an initial (arbitrary) orthogonal basis set in the l angular-momentum subspace of the correlated atomic orbitals, and using the corresponding eigenstates, which belong to a specific representation. The Hamiltonian $H^{\rm TB}(\mathbf{k})$ was evaluated on a $\mathbf{k}$-point grid in the irreducible part of the BZ. The integration, in equation (3), was performed using the analytical tetrahedron method [17], and was restricted to the irreducible part of the BZ by symmetrizing the Green's function matrix.

2.3. Technical details: QMC-DMFT computations

Computationally, the most involving part of the calculations is the evaluation of the path integral in the auxiliary-field QMC method, to solve for the local impurity Green's function [11]. The QMC method maps the interacting electron problem onto a sum of non-interacting problems by means of the Trotter discretization and Hubbard–Stratonovich transformation [11, 18]. The imaginary-time integrals are represented, in the Trotter discretization, by L imaginary-time slices of size $\Delta = \beta/L$, with $\beta = 1/K_{\rm B}T$. For an M-orbital impurity problem, the Hubbard–Stratonovich transformation introduces $M(2M-1)$ auxiliary Ising fields for each time slice. In addition to the tolerance parameter of the DMFT self-consistency, the number of time slices L and the number of Monte Carlo sweeps $N_{\rm MC}$ for the stochastic integration of the path integral are the sole convergence parameters of the QMC-DMFT calculations. It should be noted that the computational cost of the QMC algorithm scales, to the leading order in L, as $\sim M(2M-1)N_{\rm MC}L^3$ [18].

The QMC method has the advantage of having formally no approximation. Very low temperatures, however, are not accessible, as the numerical effort scales as $1/T^3$. From the imaginary-time self-consistent Green's function obtained from the QMC-DMFT computations, the real-frequency single-particle spectral functions are computed using the maximum entropy method [19].

3. Applications

The joint DMFT pseudopotential plane-wave scheme described in the previous sections was applied to two test cases, $SrVO_3$ and V_2O_3. For the density-functional calculations, we used the Perdew–Burke–Ernzerhof GGA exchange–correlation functional [20] together with Vanderbilt utrasoft pseudopotentials [21]. We used a kinetic energy cutoff of 35 Ryd (350 Ryd) for the plane-wave expansion of the electronic states (core-augmentation charge). The self-consistent calculations were performed with a (4, 4, 4) Monkhorst–Pack $\mathbf{k}$-point grid [22]. For the computation of $\mathbf{H}^{\rm TB}(\mathbf{k})$ and of the Green's functions matrix, in equation (3), we used a (10, 10,

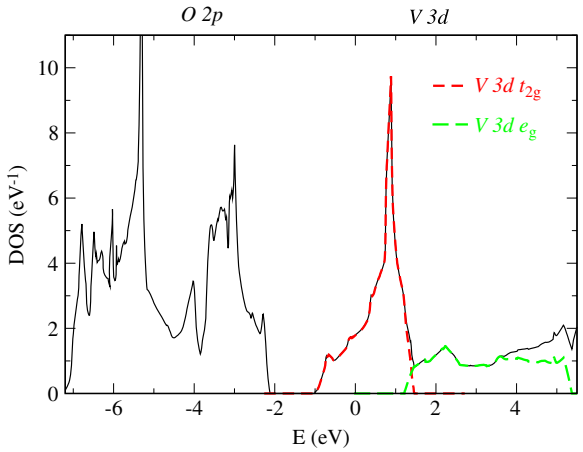

Figure 1. Density of states of $SrVO_3$ obtained from the GGA pseudopotential plane-wave calculations. The short- (long-) dashed line shows the V-3d-t_{2g} (e_g) Wannier-projected density of states. The generic characters of the bands are also indicated at the top of the figure. The zero of energy corresponds to the Fermi level.

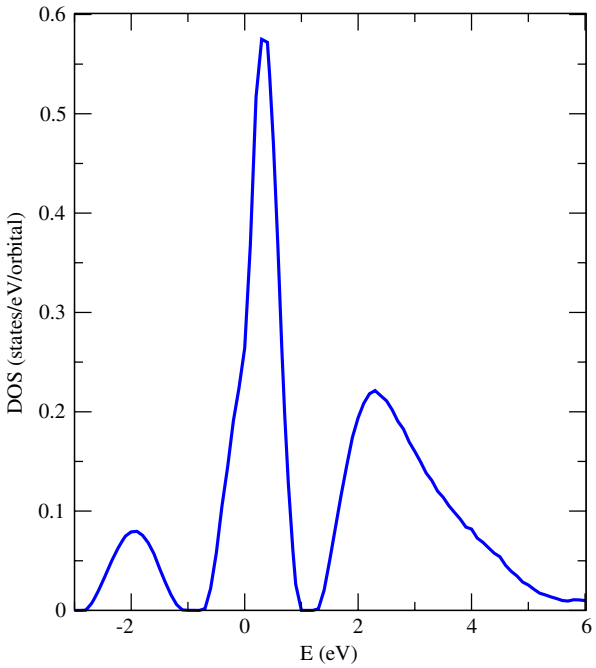

Figure 2. Spectral function for $SrVO_3$ at $T = 580$ K obtained from the GGA + DMFT computations using the t_{2g} projected Hamiltonian from the pseudopotential plane-waves calculations. The zero of energy corresponds to the Fermi level.

10) **k**-point grid centered at Γ. The experimental values of the lattice parameters of $SrVO_3$ ($a = 3.84$ Å) [23] and V_2O_3 ($a = 4.95$ Å, $c = 14.00$ Å) [24] have been used in our calculations.

For $SrVO_3$, we set the on-site Coulomb interaction $U = 5.55$ eV and Hund's rule parameter $J = 1$ eV [25]. For V_2O_3, we used $J = 0.93$ eV [24] and several different values of U [6]. The QMC-DMFT calculations were performed at $T = 580$ K ($\beta = 20$ eV^{-1}), using 80 imaginary-time slices. In the case of V_2O_3, we also performed calculations at $T = 1160$ K ($\beta = 10$ eV^{-1}), using 40 imaginary-time slices. In all QMC-DMFT calculations we used $\sim 10^6$ Monte Carlo sweeps.

3.1. $SrVO_3$

$SrVO_3$ is a prototype d^1 correlated paramagnetic metal. It has a simple cubic perovskite structure and remains paramagnetic down to low temperatures. It is an ideal test case for first-principles many-body calculations. In figure 1, we show the density of states (DOS) obtained for $SrVO_3$ from the GGA pseudopotential calculations. The spectrum is in agreement with previous LDA calculations [7, 25]. The valence states of $SrVO_3$ consist of completely occupied oxygen 2p states, located in the energy range −7 to −2 eV below the Fermi energy, and partially occupied V-3d t_{2g} states, near the Fermi energy.

From the pseudopotential plane-wave calculations, we generated the V-3d-t_{2g} and e_g Wannier functions from the Bloch functions corresponding to the five lowest-energy (3d) bands, in the energy window −1 to 5.5 eV. The corresponding projected Wannier t_{2g} and e_g DOSs are also displayed in figure 1. Because of the ideal octahedral symmetry of the V sites, hybridization is forbidden between the t_{2g} and e_g states. $\mathbf{H}^{\mathrm{TB}}(\mathbf{k})$ is hence block diagonal with respect to these two subspaces. We have used, as correlated subspace, the t_{2g} Wannier-functions subspace, and the corresponding t_{2g}-Hamiltonian block for the DMFT computations.

It should be noted that, in the special case of cubic symmetry, the Green's function matrix of the t_{2g} states, in equation (3), may be expressed as: $G_{mm'}(\epsilon) = \int \frac{\mathrm{d}\epsilon D(\epsilon')}{\epsilon - \mu - \epsilon' - \Sigma_{mm}(\epsilon')} \delta_{mm'}$. This is valid, however, only when the local matrices (self-energy and Green's function matrices) are proportional to the unitary matrix, i.e. in the case of cubic and higher symmetry. In the present work we always used the more general Hamiltonian formulation with the **k** space integration.

In figure 2, we display the corresponding single-particle spectral function obtained from the QMC-DMFT calculations at $T = 580$ K. Taking into account the correlation effects within the t_{2g} manifold leads to substantial modifications in the single-particle spectrum relative to the GGA result. Correlation effects are responsible for a lower Hubbard band around −2 eV, an upper Hubbard around 2.5 eV, and a well-pronounced quasiparticle peak at the Fermi energy. This is in general agreement with the photoemission and inverse photoemission experiments on $SrVO_3$ [26]. The results in figure 2 compare well with previous LMTO-based LDA + DMFT computations performed with the same value of U [25], and are also consistent with the mixed-basis LDA + DMFT calculations using somewhat smaller values of U [7].

3.2. V_2O_3

V_2O_3 is a vanadium d^2 system. The high-temperature paramagnetic phase of V_2O_3 has a corundum trigonal crystal structure, with four equivalent V sites in the unit cell. Within the corundum structure, each V ion is surrounded by a distorted oxygen octahedron [27, 28]. The V ions are arranged in pairs

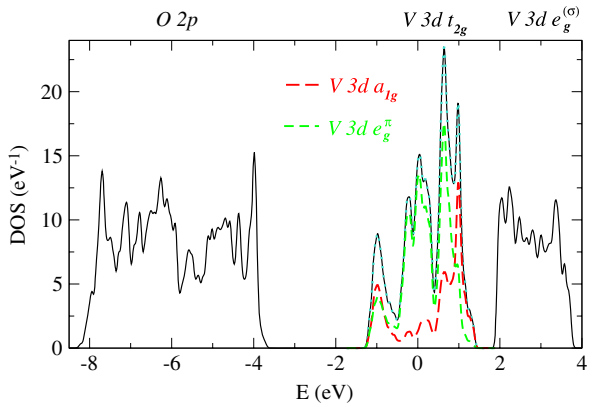

Figure 3. Density of states of V_2O_3 obtained from the GGA pseudopotential plane-wave calculations. The short- (long-) dashed line shows the V-3d-e_g^{π} (a_{1g}) Wannier-projected density of states. The generic characters of the bands are also indicated at the top of the figure. The zero of energy corresponds to the Fermi level.

along the *c* axis, with a stacking that can be obtained, starting from an ideal chain of V ions along **c**, by introducing vacancies at every third site [24]. While the V–V pairs along the *c* axis are surrounded by face-sharing oxygen octahedra, in the **a**–**b** plane, each V ion has three nearest neighbors with edge-sharing oxygen octahedra [27].

Assuming ideal V octahedral sites in V_2O_3, the V-3d atomic states are split into t_{2g} and e_g orbitals, where the two degenerate e_g orbitals are empty and the three degenerate t_{2g} orbitals are filled with two electrons. When the symmetry is further reduced by a small trigonal distortion of the octahedra in the corundum structure, the t_{2g} orbitals further split into a non-degenerate a_{1g} orbital oriented along the *c* axis, and two degenerate e_g^{π} orbitals oriented predominantly in the **a**–**b** plane.

In figure 3, we show the DOS of V_2O_3 obtained from the GGA pseudopotential calculations. The oxygen 2p states of V_2O_3 are located roughly between -8 and -4 eV below the Fermi energy. The V-3d t_{2g}-like states are located in an energy window between -1.5 and 1.5 eV, and the e_g^{σ} states are approximatively between $\sim$2 and 4 eV. This is consistent with previous LDA calculations [24, 28, 29]. The GGA (and also LDA) calculations yield a metallic phase for V_2O_3, with a high DOS at the Fermi energy.

We generated Wannier functions with a_{1g} and e_g^{π} symmetry from the Bloch states enclosed in the energy window -1.5 to 1.5 eV (see figure 3). The corresponding Wannier-projected DOSs are also displayed in figure 3. We used these Wannier functions to construct $\mathbf{H}^{\mathrm{TB}}(\mathbf{k})$ and carry out the GGA + DMFT computations. The results are shown in figures 4 and 5 for two different temperatures: $T = 1160$ K and 580 K, respectively. The separate a_{1g} and e_g^{π} contributions to the spectral function are displayed in the upper and lower panels, respectively. At $T = 1160$ K, calculations were performed for $U = 5.6$ and 6 eV. An insulating phase is obtained for $U = 6$ eV, while the system is still metallic at $U = 5.6$ eV. The results in figure 4 agree well with the available LMTO-based LDA + DMFT calculations performed

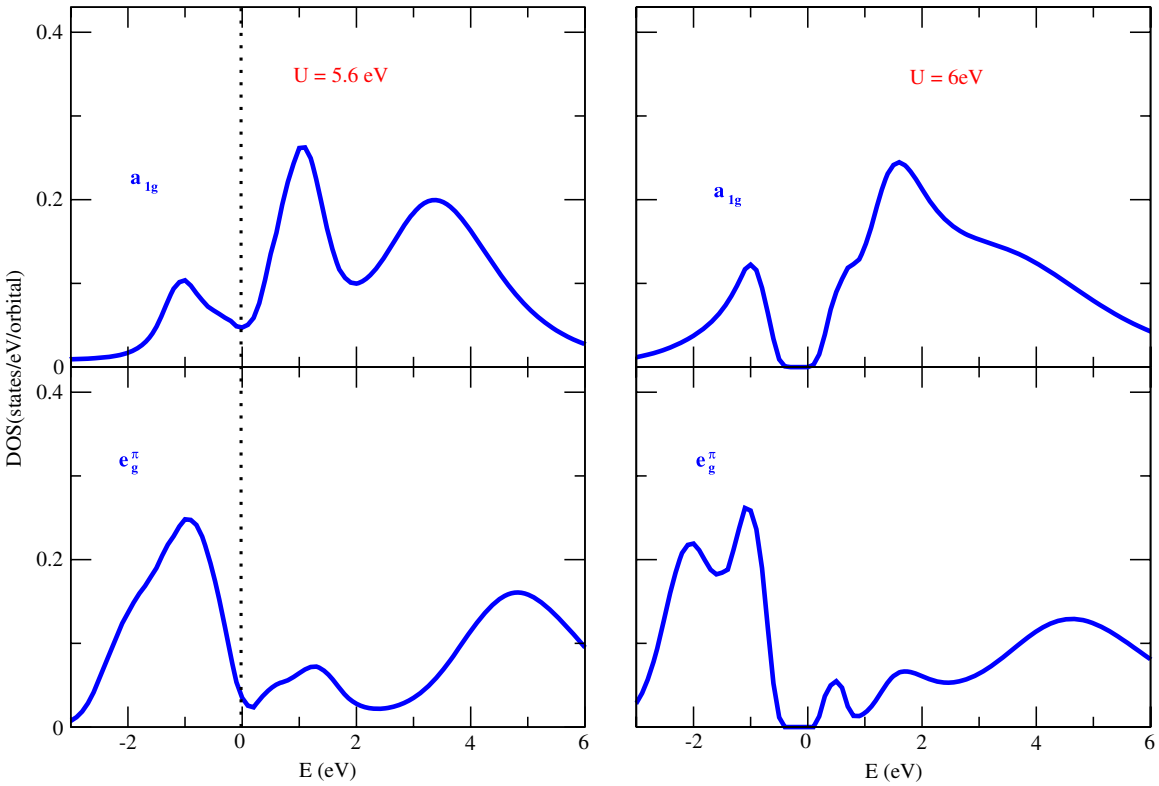

Figure 4. V-3d a_{1g} and e_g^{π} contributions to the spectral function of V_2O_3 at $T = 1160$ K, as obtained from the GGA + DMFT computations using the t_{2g}-like Hamiltonian constructed from the pseudopotential plane-wave calculations. The results are shown for two different values of the on-site Coulomb interaction, $U = 5.6$ and 6 eV. The vertical dotted line indicates the Fermi energy.

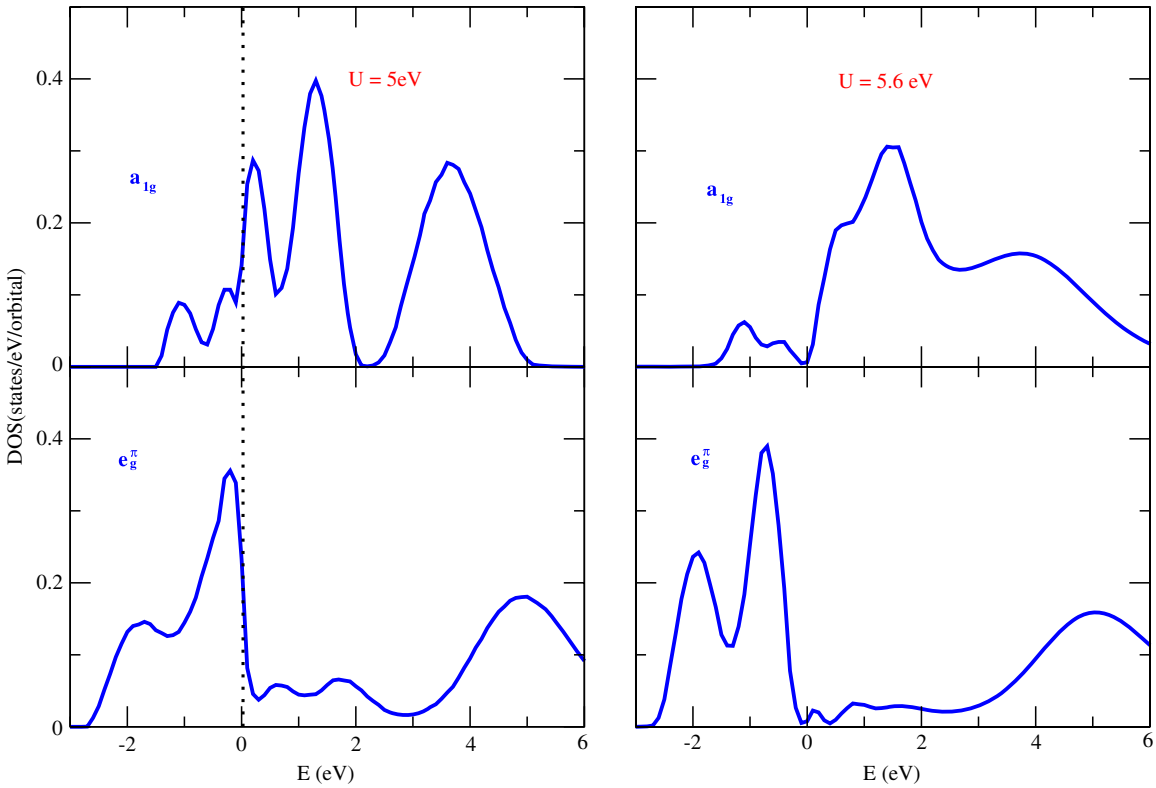

Figure 5. Same data as in figure 4, but for $T = 580$ K and $U = 5$ and 5.6 eV.

at the same temperature [6, 24, 29], and in particular with the results obtained using a Wannier-projected Hamiltonian [6]. The pseudopotential implementation is found to yield a slightly larger critical U for the insulating phase ($U \sim 6$ eV) compared to the LMTO implementation ($U \sim 5.5$ eV) [6]. This is related to the bandwidth of the LDA/GGA t_{2g}-like states, which is slightly larger in the pseudopotential case compared to the LMTO case.

At $T = 580$ K, we performed calculations for $U = 5$ and 5.6 eV. An insulating phase is found at $U \sim 5.6$ eV, whereas at $U = 5$ eV the system is metallic, with a large DOS at the Fermi energy. In the latter case, one observes a quasiparticle peak at the Fermi energy in the a_{1g} orbital-resolved spectral function. The results at $T = 580$ K, in figure 5, are in good qualitative agreement with the results of LDA + DMFT calculations using a Wannier Hamiltonian constructed with the Nth order muffin-tin-orbital method [30]. In the latter study, a critical U of 4.2 eV was found for the insulating phase. The larger critical U obtained here (5.6 eV) is attributed mainly to the difference in the crystal structure. In [30] the $(V_{0.962}Cr_{0.038})_2O_3$ crystal structure was considered, which corresponds to the experimental insulating structure. The increased U is also due in part to the broader GGA band found in the pseudopotential calculations. One observes also some small differences in the peak structure, between the present results in figure 5 and the spectral function in [30]. These are attributed mainly to differences in the DMFT calculational details, such as the use of two different interpolation schemes (Ulmke–Janis–Vollhardt scheme [31] versus cubic splines) for the Fourier transformation of the local Green's function in the two studies.

3.3. Discussion and outlook

The results we have presented here show that the DMFT plus pseudopotential plane-wave scheme is both a practical and suitable approach for the determination of the electronic properties of strongly correlated oxides. A promising extension of this approach concerns the determination of total-energy properties, and in particular of structural properties of correlated systems. The total energy, within the LDA + DMFT, can be expressed as [32]: $E = E_{\mathrm{LDA}} - E_{\mathrm{DC}} - \sum_{m,\mathbf{k}} \epsilon^{\mathrm{LDA}}_{m,\mathbf{k}} + \langle H^{\mathrm{TB}}_{\mathrm{LDA}} \rangle + \langle H_U \rangle$, where E_{LDA} is the LDA total energy, E_{DC} is the double-counting energy corresponding to the second term on the right-hand side of equation (2), $\sum_{m,\mathbf{k}} \epsilon^{\mathrm{LDA}}_{m,\mathbf{k}}$ is the sum of the LDA valence-state eigenvalues, $\langle H^{\mathrm{TB}}_{\mathrm{LDA}} \rangle = \mathrm{tr}[\mathbf{H}^{\mathrm{TB}}\mathbf{G}]$, and $\langle H_U \rangle$ is the interaction energy, corresponding to the third and fourth terms on the right-hand side of equation (2), computed from the double occupancy matrix [33]. The application of the DMFT pseudopotential plane-wave approach to the determination of structural relaxations is a line of development we are currently pursuing.

4. Summary and conclusions

We have presented an implementation of the LDA + DMFT approach within the pseudopotential plane-wave framework.

This scheme was applied to two different test cases, $SrVO_3$ and V_2O_3. Comparison with available LMTO-based LDA + DMFT calculations demonstrated the suitability of the joint DMFT pseudopotential plane-wave scheme to describe the electronic properties of strongly correlated materials. This opens the way to future developments using the DMFT pseudopotential plane-wave approach to address total-energy and hence structural properties of correlated systems.

Acknowledgments

We thank S de Gironcoli, M Altarelli, and D Vollhardt for helpful discussions. We are also grateful to D Vollhardt for providing the QMC-DMFT code. We acknowledge support for this work from the Light Source Theory Network, LighTnet, of the EU. Calculations were performed on the IBM sp5 computer at CINECA.

References

[1] See, e.g. Dagotto E 2005 *Science* **309** 257
[2] See, e.g. Tokura Y and Nagaosa N 2000 *Science* **288** 462
[3] Kotliar G and Vollhardt D 2004 *Phys. Today* **57** (3) 53
[4] Anisimov V I, Poteryaev A I, Korotin M A, Anokhin A O and Kotliar G 1997 *J. Phys.: Condens. Matter* **9** 7359
[5] Lichtenstein A I and Katsnelson M I 1998 *Phys. Rev.* B **57** 6884
[6] Anisimov V I, Kondakov D E, Kozhevnikov A V, Nekrasov I A, Pchelkina Z V, Allen J W, Mo S-K, Kim H-D, Metcalf P, Suga S, Sekiyama A, Keller G, Leonov I, Ren X and Vollhardt D 2005 *Phys. Rev.* B **71** 125119
[7] Lechermann F, Georges A, Poteryaev A, Biermann S, Posternak M, Yamasaki A and Andersen O K 2006 *Phys. Rev.* B **74** 125120
[8] Pavarini E, Biermann S, Poteryaev A, Lichtenstein A, Georges A and Andersen O K 2004 *Phys. Rev. Lett.* **92** 176403
[9] Kunes J, Anisimov V I, Lukoyanov A V and Vollhardt D 2007 *Phys. Rev.* B **75** 165115
[10] Fresard R and Kotliar G 1997 *Phys. Rev.* B **56** 12909
[11] Georges A, Kotliar G, Krauth W and Rozenberg M J 1996 *Rev. Mod. Phys.* **68** 12
[12] Hirsch J E and Fye R M 1986 *Phys. Rev. Lett.* **56** 2521
[13] Ku W, Rosner H, Pickett W E and Scalettar R T 2002 *Phys. Rev. Lett.* **89** 167204
[14] Marzari N and Vanderbilt D 1997 *Phys. Rev.* B **56** 12847
[15] Baroni S, dal Corso A, de Gironcoli S and Giannozzi P URL http://www.pwscf.org/ the pwscf package is part of the Quantum Espresso package and URL:http://www.quantum-espresso.org/
[16] Cococcioni M and de Gironcoli S 2005 *Phys. Rev.* B **71** 35105
[17] Lambin Ph and Vigneron J P 1984 *Phys. Rev.* B **29** 3430
Jepsen O and Andersen O K 1971 *Solid State Commun.* **9** 1763
Blöchl P E, Jepsen O and Andersen O K 1994 *Phys. Rev.* B **49** 16223
[18] Held K, Nekrasov I A, Keller G, Eyert V, Blümer N, McMahan A K, Scalettar R T, Pruschke T, Anisimov V I and Vollhardt D 2002 *Quantum Simulations of Complex Many-Body Systems: From Theory to Algorithms* (*NIC Series* vol 10) (Jülich: John von Neumann Institute for Computing)
[19] Jarrell M and Gubernatis J E 1996 *Phy. Rep.* **269** 133
[20] Perdew J P, Burke K and Ernzerhof M 1996 *Phys. Rev. Lett.* **77** 3865
[21] Vanderbilt D 1990 *Phys. Rev.* B **41** 7892
[22] Monkhorst H J and Pack J D 1976 *Phys. Rev.* B **13** 5188
[23] Reya M J, Dehaudta Ph, Joubertb J C, Lambert-Andronc B, Cyrotd M and Cyrot-Lackmanne F 1990 *J. Solid State Chem.* **86** 101
[24] Keller G, Held K, Eyert V, Vollhardt D and Anisimov V I 2004 *Phys. Rev.* B **70** 205116 and references therein
[25] Nekrasov I A, Keller G, Kondakov D E, Kozhevnikov A V, Pruschke Th, Held K, Vollhardt D and Anisimov V I 2005 *Phys. Rev.* B **72** 155106
[26] Sekiyama A, Fujowara H, Imada S, Suga S, Eisaki H, Uchida S I, Takegahara K, Harima H, Saitoh Y, Nekrasov I A, Keller G, Kondakov D E, Kozhevnikov A V, Pruschke Th, Held K, Vollhard D and Anisimov V I 2004 *Phys. Rev. Lett.* **93** 156402
Morikawa K, Mizokawa T, Kobayashi K, Fujimori A, Eisaki H, Uchida S, Iga F and Nishihara Y 1995 *Phys. Rev.* B **52** 13711
[27] Tanaka A 2002 *J. Phys. Soc. Japan* **71** 1093
[28] Hébert C, Willinger M, Su D S, Pongratz P, Schattschneider P and Schlögl R 2002 *Eur. Phys. J.* B **28** 407
[29] Held K, Keller G, Eyert V, Vollhard D and Anisimov V I 2001 *Phys. Rev. Lett.* **86** 5345
[30] Poteryaev A I, Tomzcak J M, Biermann S, Georges A, Lichtenstein A I, Rubtsov A N, Saha-Dasgupta T and Andersen O K 2007 *Phys. Rev.* B **76** 85127
[31] Ulmke M, Janis V and Vollhardt D 1995 *Phys. Rev.* B **51** 10411
[32] Amadon B, Biermann S, Georges A and Aryasetiawan F 2006 *Phys. Rev. Lett.* **96** 66402
Held K, McMahan A K and Scalettar R T 2001 *Phys. Rev. Lett.* **87** 276404
[33] McMahan A K 2005 *Phys. Rev.* B **72** 115125